Complementary Roles of Human Hippocampal Subfields in Differentiation and Integration of Spatial Context

Jared Stokes, Colin Kyle, and Arne D. Ekstrom

Abstract

■ The unique circuitry of the hippocampus is thought to support the encoding and retrieval of context-rich episodic memories. Given the neuroanatomical differences between the hippocampal subfields, determining their functional roles during representation of contextual features in humans is an important yet unaddressed research goal. Prior studies suggest that, during the acquisition of information from the environment, the dentate gyrus (DG) and CA3 subfields rapidly differentiate competing contextual representations, whereas CA1, situated downstream from CA3/DG, is believed to process input from both CA3 and neocortical areas via the temporoammonic pathway. To further explore the functionality of these roles, we used high-resolution fMRI to investigate multivariate response patterns within CA3/DG and CA1 during the processing of spatial context. While undergoing functional imaging, participants viewed videos of virtual environments and were asked to discriminate between similar yet geometrically distinct cities. We manipulated a single contextual feature by systematically morphing the city configurations from one common geometric shape to another, resulting in four cities—two distinctively shaped cities and two intermediate "morphed" cities. Pattern similarity within CA3/DG scaled with geometric changes to the environment. In contrast, CA1 pattern similarity, as well as interregional pattern similarity between CA1 and parahippocampal cortex, increased for the regularly shaped configurations compared with the morphs. These results highlight different roles for subfields CA3/DG and CA1 in memory and advance our understanding of how subcomponents of the human hippocampal circuit represent contextual features of memories. ■

INTRODUCTION

The hippocampus plays a critical role in representing contextual details that underlie our memory for events (Diana, Yonelinas, & Ranganath, 2007; Eichenbaum, Yonelinas, & Ranganath, 2007; Smith & Mizumori, 2006; Yonelinas, Kroll, Dobbins, Lazzara, & Knight, 1998). Part of this role is widely assumed to involve binding features of an event to a specific spatial context (memory for "where" something occurred, such as at a café), referred to more generally as memory for context (Diana et al., 2007; Tulving, 2002). Yet, how the human hippocampus represents and differentiates spatial context during episodic memory encoding and retrieval remains largely unknown. Given the hypothesized importance of the primary hippocampal subfields, CA3, CA1, and dentate gyrus (DG; Amaral & Witter, 1989), to aspects of episodic memory performance (Yassa & Stark, 2011; Katz, Kath, Spruston, & Hasselmo, 2007; Rolls & Kesner, 2006; Guzowski, Knierim, & Moser, 2004), determining what roles the different subfields play when processing spatial context in humans remains critical in advancing our understanding of the neural basis of memory.

Anatomical tracing studies suggest differences between afferent input to CA3 and CA1; specifically, a significant percentage of CA3 input comes from its recurrent collaterals, whereas the primary sources of CA1 input come from both CA3 and neocortical areas (via the temporoammonic pathway; Amaral & Insausti, 1990). Thus, because of the recurrent collaterals, CA3/DG would appear best suited to complete/differentiate competing inputs (Levy, 1989), whereas CA1 may be in a unique position to combine differentiated input from CA3 and generalized input from neocortical areas (van Kesteren, Ruiter, Fernandez, & Henson, 2012; Katz et al., 2007), such as parahippocampal and retrosplenial cortex. Therefore, we might predict that CA3/DG and CA1 would show distinct roles in the representation of spatial context during the formation of memories.

Although past studies have identified differences in subfield activation during verbal and object-related memory (Brown, Hasselmo, & Stern, 2014; Lacy, Yassa, Stark, Muftuler, & Stark, 2010; Bakker, Kirwan, Miller, & Stark, 2008; Kirwan, Jones, Miller, & Stark, 2007; Zeineh, Engel, Thompson, & Bookheimer, 2003; Zeineh, Engel, & Bookheimer, 2000), these studies were not designed to examine how the subfields represent spatial context, a critical component of episodic memory. Furthermore, because rodent studies have suggested segregated input of spatial and nonspatial context into the hippocampus via entorhinal cortex (EC) (Hargreaves, Rao, Lee, & Knierim, 2005) and different coding schemes for spatial versus nonspatial information within the hippocampus (Leutgeb et al., 2005), it is important to establish how and in what manner spatial context is processed within the human hippocampal subfields.

University of California, Davis

Journal of Cognitive Neuroscience 27:3, pp. 546–559
doi:10.1162/jocn_a_00736

To address this question, we scanned participants as they performed a contextual discrimination task, which involved viewing immersive video clips from four distinct virtual reality cities. We employed high-resolution fMRI to target the hippocampus and utilized multivariate pattern similarity (MPS) analyses (Kriegeskorte & Bandettini, 2007; Kriegeskorte, Goebel, & Bandettini, 2006) to examine internal contextual representation within the hippocampal subfields. Both patient and neuroimaging studies have demonstrated the importance of the hippocampus in tasks involving spatial scene perception, allocentric processing, and spatial memory (Barense, Henson, Lee, & Graham, 2010; Hartley et al., 2007; Graham et al., 2006; Astur, Taylor, Mamelak, Philpott, & Sutherland, 2002; King, Burgess, Hartley, Vargha-Khadem, & O'Keefe, 2002). By inducing small systematic manipulations to the boundary shape of the virtual cities (i.e., morphing from a circle to a square), we were able to examine the response sensitivity to parametric changes to spatial context. In accordance with prior work in rodents using a related paradigm (Leutgeb et al., 2005; Wills, Lever, Cacucci, Burgess, & O'Keefe, 2005), we hypothesized that CA3/DG and/or CA1 would show parametric changes in neural representations as a function of geometric dissimilarity. Second, we tested for subfield differences in the trial-to-trial representation of regular geometries (circle, square) in comparison with the perceptually ambiguous morph-shaped cities, based on the hypothesis that CA1 might serve as a locus of integration of stored geometrical templates (i.e., regular cities) represented in neocortical regions (Op de Beeck, Wagemans, & Vogels, 2001) with input from CA3 (Remondes & Schuman, 2004). Our results provide novel evidence that hippocampal subfields serve distinct roles during the extraction of spatial contextual details and assimilation of these details with preexisting cortical representations of shapes in support of episodic memory.

METHODS

Participants

Seventeen participants (10 women) were recruited from the University of California-Davis community. All participants were native English speakers with normal or corrected-to-normal vision between the ages of 18 and 30 years. Each volunteer was paid for the entire session, which lasted approximately 3 hr. All participants gave informed written consent before participation. One participant was removed from the study because of excessive head movement in the scanner.

Task Design

Four virtual environments were constructed using the Unity software package (San Francisco, CA). We modeled a "morphed" design manipulation used in past rodent studies (Leutgeb et al., 2005; Wills et al., 2005) by systematically varying the positioning of eight unique stores to produce four cities arranged along a circle–square spectrum (Figure 1B). Two of these configurations were a square-shaped and circular-shaped layout (City 1 and City 4, respectively). The other two cities were circle–square and square–circle morphs (City 2 and City 3, respectively; Figure 1A). Whereas city configurations involved a progressive transformation between circle and square, we held landmark identity and ordinal position constant.

Store positions were calculated using the Matlab function polymorph (www.mathworks.com). Each polygon contained eight points, which were shifted approximately

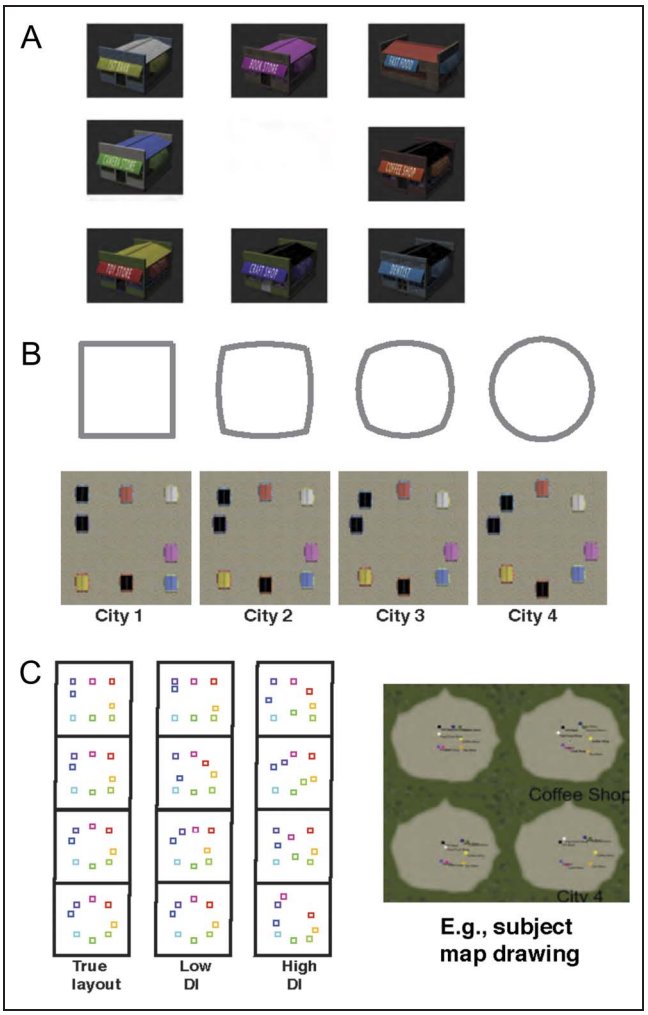

Figure 1. Virtual reality spatial discrimination paradigm. (A) Each city contained an identical set of eight stores (first bank, book store, fast food, camera store, coffee shop, toy store, craft shop, and dentist). Before the start of the experiment, each participant previewed the storefronts in a series of three video montages. (B) Aerial view of the four geometrically morphed virtual cities shows how the city store positions change as a function of morphing for the four different cities. (C) After the context discrimination task (i.e., scanner task), participants performed the postscan map-drawing task. Lower MDI indicates more accurate map drawings.

equal distance between neighboring morphs. For instance, the Euclidean distance shift between the position of Store A in City 1 and its position in City 2 was equivalent to the distance between the position of Store B in City 1 and Store B's position in City 2 (Figure 1A). Consequently, in this example, the total Euclidean distance calculated from point shifts from City 1 to City 2 was equal to the total distance between City 2 and City 3.

First-person navigation video clips were recorded within the cities, with each video clip (20 sec long) corresponding to a single trial. Each video was captured from a single city (Figure 1A and B), and all video clips contained a unique, nonrepeated navigation route.

Behavioral Methods

Participants were presented video clips in the scanner and were explicitly told to study the environment and attempt to mentally extract the city configuration. To ensure that attention was focused on the city geometry, we asked participants to compare the geometric configuration of the current trial to the configuration from the prior video trial in a manner similar to continuous recognition paradigms (e.g., Viskontas, Knowlton, Steinmetz, & Fried, 2006). The cities were designed to require the participants to assess the configuration holistically rather than approximate the geometry of the city based on a single view, which we determined during behavioral piloting. After the first trial of each run, participants indicated with a button press whether the current city was the "same" or "different" than that of the former trial. Beforehand, participants were explicitly instructed that each city contained an identical set of eight stores ("first bank," "book store," "camera store," "coffee shop," "toy store," "craft shop," "dentist," and "fast food shop"). Participants were also informed that the ordinal sequence of the stores would remain constant across cities but that each city would possess a different geometric configuration.

On the first trial of each run, participants were instructed to simply watch the video clip and try to learn the city layout. On successive trials, participants were asked to make a button box response: "Press button 1 if you believe the city depicted in the video is the same as the city depicted in the video, which occurred immediately prior, and press button 2 if you believe it to be a different city." Participants were instructed to make a response within the 20-sec time frame of the video and process the spatial information provided in the clip after making a response. Between trials, participants performed a 5-sec-long active baseline task to reduce rest-related activity within the medial-temporal lobe (Stark & Squire, 2001), which consisted of an arrow pointing either left or right; participants pressed Button 1 for left or Button 2 for right. A total of 96 video clips were divided across four runs, and after omitting the opening trial, we collected 92 trials of interest from each participant.

Participants were explicitly told that there were four cities but were given no other descriptive information about the configurations of the cities (i.e., circle or square). Immediately after the scan, we evaluated participant knowledge of the spatial geometries of each city by asking participants to construct maps (Wolbers & Buchel, 2005) of the four cities as accurately as possible using in-house map-drawing software (Figure 1C). Each map was then oriented by store serial order and projected into template space through affine transformation. All except a single participant correctly recalled store serial order; this participant simply transposed two of the stores. To assess city geometry accuracy, we calculated the ratio of map-to-template area difference to total template area (distortion index) for each city. Distortion indices were used to ascertain which maps corresponded to the square city (City 1) and circle city (City 4). Next, scores of the remaining maps were used to match participant drawings to square-morph city (City 2) and circle-morph city (City 3). We then created a single composite map-drawing distortion index (MDI) score for the purposes of assessing overall map-drawing performance. Because several participants were only able to recall three city maps, their morph-city MDI scores were calculated using a single morph city map.

Trials were presented in pseudorandomized order that ensured an equal distribution of same and different trials (46 same and 46 different trials), equal numbers of environment type (City 1, City 2, City 3, and City 4; 23 trials each), and equal numbers of city pair combinations (e.g., City 1 followed by City 2, City 2 followed by City 3, etc.). Run order was counterbalanced across participants. Both the scan task and map-drawing task were programed and employed through the Psychophysics Toolbox (psychtoolbox.org/).

Outside the scanner, each participant successfully completed a practice module, which consisted of mock versions of both the continuous recognition and map-drawing tasks. Before beginning the experiment, participants were first acclimated to the serial order of the city configuration by viewing a video montage containing 360° rotating presentations of each of the eight stores on a black background within the scanner. The temporal order of this montage matched the serial order of stores along the city perimeters. The purpose of the acclimation phase was to ensure heightened processing of city configuration over that of store order and descriptor information during task.

fMRI Methods

Participants were scanned at the University of California-Davis Imaging Center in Davis, CA, using a Siemens 64-channel 3-T "Skyra" MRI System (Munich, Bavaria). Sequences were acquired perpendicular to the long axis of the hippocampus. High-resolution functional (BOLD) images were collected using an EPI sequence (repetition time [TR] = 3000 msec,

echo time [TE] = 29 msec, slices = 36, field of view [FOV] = 192 mm, bandwidth = 1462 Hz/pixel, resolution = 1.5 × 1.5 × 2 mm). High-resolution structural images were acquired using a T2-weighted turbo-spin echo sequence (TR = 4200 msec, TE = 93 msec, FOV = 20 cm, flip angle = 139°, bandwidth = 199 Hz/pixel, voxel size = 0.4 × 0.4 × 1.9 mm). In addition, coplanar matched-bandwidth EPI sequences (TR = 3000 msec, TE = 38 msec, slices = 36, FOV = 245 mm, flip angle = 90°, bandwidth = 1446 Hz/pixel) were collected and utilized to improve registration of the EPI images to the high-resolution structural scan (Ekstrom et al., 2009; Zeineh et al., 2000).

The functional images were slice-time and head-motion corrected using SPM8 (www.fil.ion.ucl.ac.uk/spm/). The coplanar matched-bandwidth structural scan was coregistered to the mean of the realigned functional scans. Subsequently, the T2 high-resolution image was then coregistered to the matched-bandwidth image. Individual trial responses were estimated using a voxel-wise, general linear model that produced a summary image for each of the 92 trials of interest. Specifically, each trial (i.e., a 20-sec video period) was entered as a regressor, which then allowed for the resulting trial-specific beta images to be sorted by condition (e.g., S-ALL, D-ALL) and statistically compared. Each model incorporated movement and run information as nuisance regressors.

We constrained our analyses to the medial temporal lobe (MTL) and targeted the following areas commonly implicated in spatial context representation (Eichenbaum et al., 2007): CA1, CA3, DG, and the extrahippocampal parahippocampal cortex (PHC; Figure 1). EC was omitted from analyses because of imaging signal dropout, an issue present in other high-resolution imaging studies targeting the MTL using similar MRI acquisition sequences (e.g., Duncan, Tompary, & Davachi, 2014). In accordance with the methodology from other high-resolution fMRI projects, the "CA3/DG" ROI was defined to include subfields CA3, CA2, and DG because spatial resolution limitations prevent finer division (LaRocque et al., 2013; Chen, Olsen, Preston, Glover, & Wagner, 2011; Ekstrom et al., 2009; Zeineh et al., 2000). Boundaries of these regions were traced by hand on the T2-weighted turbo-spin echo structural scans using the "FSLview" module of FSL (fsl.fmrib.ox.ac.uk/fsl/fslwiki/) and following guidelines similarly utilized in past reports (Ekstrom et al., 2009; Zeineh et al., 2000; Duvernoy, 1998). For the group searchlight analysis, participant-specific information maps were warped into a common space. Cross-participant alignment was achieved using diffeomorphic metric mapping method and implementing participant-specific weighted ROIs. All procedures were carried out in Matlab with in-house scripts that employed the Advanced Normalization Tools framework (Avants, Epstein, Grossman, & Gee, 2008). Normalization procedures warped all participants' T2 images to that of a template participant and used the resulting deformation maps to additionally carry along all information maps into common space. These morphed maps were then subjected to one of three types of group analysis: contrast, linear trend analysis, and seed-based interregional pattern coherence (IRPC) analysis. The searchlight analysis involved extracting voxel-wise MPS scores within the searchlight sphere, which was conducted for each condition of interest within each participant. We established significant clusters by thresholding at a value of two-tailed $p < .05$ and at a minimum of four contiguous voxels (determined through permutation testing to exceed the false positive rate at $p < .05$ [corrected]; Forman et al., 1995).

Both ROI and searchlight analyses utilized a metric of neural similarity, MPS, congruent with the representational similarity analysis approach (Kriegeskorte et al., 2006). Neural activation patterns were defined for each of the 92 trials of each participant using general linear model estimates. All trials were analyzed regardless of response accuracy; however, no-response trials were excluded. MPS was calculated on a trial-by-trial basis by correlating ROI-bound voxel patterns for each pair of neighboring trials (i.e., 4 runs × 23 = 92 pattern similarity scores in total). Outliers were controlled for at the voxel level by replacing extreme values with ROI mean values and, in addition, at the MPS level, by omitting extreme scores greater than 1.5 × the interquartile range. Trial-wise MPS was approximated using Pearson correlations of voxelwise BOLD activity between temporally adjacent pairs of trials (Figure 2B). Fischer z transforms were employed on correlation values when entered into all statistical tests (Fischer, 1928). MPS was calculated within ROI in the ROI-centric analysis, and in the searchlight analysis, MPS was calculated within a three voxel-wide radius pseudospherical shape chosen to accommodate the protracted dimensions of the human MTL. In both cases, MPS scores were parsed by behavioral conditions (all same trials [S-ALL], all different trials [D-ALL], different trials differing by one morph [D-1], different trials differing by two morphs [D-2], same City 1 and 4 trials [S-C1&4], and same City 2 and 3 trials [S-C2&3]; Figure 2A) and averaged within participant. Participants responded substantially faster to cities differing by at least three geometrical morph iterations (D-3) versus all other city comparisons (D-3: 7.57 sec [1.83] vs. D-1: 13.47 sec [2.4], D-2: 10.85 sec [2.08], and S-ALL: 14.37 sec [1.97]). D-3 judgments also was only composed of a small number of trials ($N = 7$). Thus, we did not include D-3 city comparisons in our final analyses, although including them did not change our results significantly overall.

IRPC was calculated for each participant by computing Pearson's r between each node and each seed of interest (CA1 and CA3/DG) using the fluctuating trial-to-trial MPS scores, parsed by condition of interest (i.e., S-C1&4 and S-C2&3). The analysis is similar to a beta series functional connectivity analyses (Rissman, Gazzaley, & D'Esposito, 2004), and although somewhat novel, a similar technique was effectively implemented in a prior study to assess hippocampal–cortical pattern similarity coherence (Ritchey, Yonelinas, & Ranganath, 2014).

RESULTS

Behavioral Performance

All participants discriminated the spatial configurations significantly above chance (accuracy = 73% [standard deviation (*SD*) = 12%]) and, overall, displayed higher accuracy when judging two trials as different compared with identification of trials as same (S-ALL: 68% correct [*SD* = 16%]; D-ALL: 79% correct [*SD* = 11%]; $t(15) = 3.57$, $p = .0028$). D-prime (d') scores, which account for participants using more conservative or liberal strategies to disambiguate same/different cities (Macmillan & Creelman, 2005), were also significantly greater than chance (mean $d' = 1.37$ (0.80); $t(15) = 6.83$, $p < .0001$) and did not vary as a function of learning over the course of experimental runs (repeated-measures one-way ANOVA: $F(3, 42) = 1.7$, $p = .181$). Consistent with the idea that participants actively processed differences in spatial geometry of the cities, performance varied as a function of increasing geometrical dissimilarity (d' D-1 = 0.96 (0.76); d' D-2 = 1.52 (1.03); d' D-3 = 1.54 (.71); $F(2, 30) = 17.83$, $p < .0001$). This indicated that the greater the geometrical dissimilarity, the greater the ability of participants to discriminate cities as different. In addition to detecting geometrically different cities more readily, participants also drew maps of regular cities (Cities 1 and 4) more accurately than morph cities (Cities 2 and 3; Figure 1B and D). Specifically, participants' MDIs (excluding one outlier participant [*Z* score = 3.68]) revealed a significant difference in MDI between the four cities ($F(3, 42) = 10.48$, $p < .0001$), with post hoc comparisons showing that the MDI for morph cities was higher than that for regular cities (Table 1). In summary, our behavioral results indicate that participants were readily able to discriminate same and different cities, that this ability varied as a function of differences in spatial geometry, and that morphed cities resulted in less stable representations than geometrically regular cities.

Table 1. Participants Successfully Detected Change in Context

	M	*SD*
Behavioral Results		
Discrimination task		
Same (CRT)	0.68	0.16
Different (CRT)	0.79	0.11
S-C1&4 (CRT)	0.73	0.14
S-C2&3 (CRT)	0.62	0.19
d'	1.37	0.80
Map drawing		
DI–C1	0.0832	0.0503
DI–C2	0.1238	0.0586
DI–C3	0.1409	0.0573
DI–C4	0.1071	0.0478

Detecting change in context (different trials) resulted in higher performance than detecting preservation of context (same trials). Performance was also higher for same Cities 1 and 4 trials (S-C1&4) compared with same Cities 2 and 3 (S-C2&3). Importantly, in all conditions, participants performed significantly above chance levels. To assess spatial learning, participants were asked to create maps of each of the four cities. Mean DI scores describe the overall amount of map-drawing distortion.

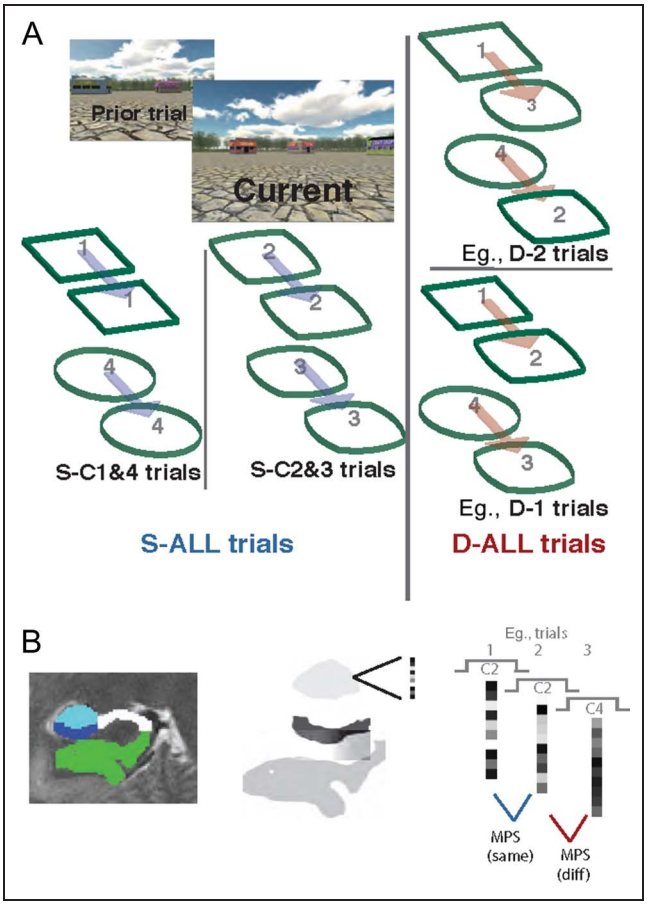

Figure 2. Experimental conditions and pattern similarity analysis. (A) The same trials (S-ALL) were broken down into specific conditions by degree of geometric regularity. S-C1&4 (i.e., square, circle) condition embodied recognizable regular geometric templates when compared with the S-C2&3 trials, which involved morphed geometric shapes (i.e., City 2: square–circle; City 3: circle–square). Different trials (D-ALL) were further parsed by degree of discrimination difficulty, which scaled with between-city geometric similarity. Therefore, cities involved in D-1 trials were more easily discriminated than D-2 trials. (B) Subfields were manually traced and included CA3/DG (teal), CA1 (blue), and PHC (green). MPS analysis was utilized to compare adjacent trials and generate trial-specific pattern similarity scores.

A Role for CA3/DG in Differentiating Same from Different Spatial Contexts

We performed an ROI analysis on MPS values to assess sensitivity to change in environmental input in subfields CA3/DG, CA1, and PHC. We identified a single subfield within the hippocampus showing differences in MPS as a

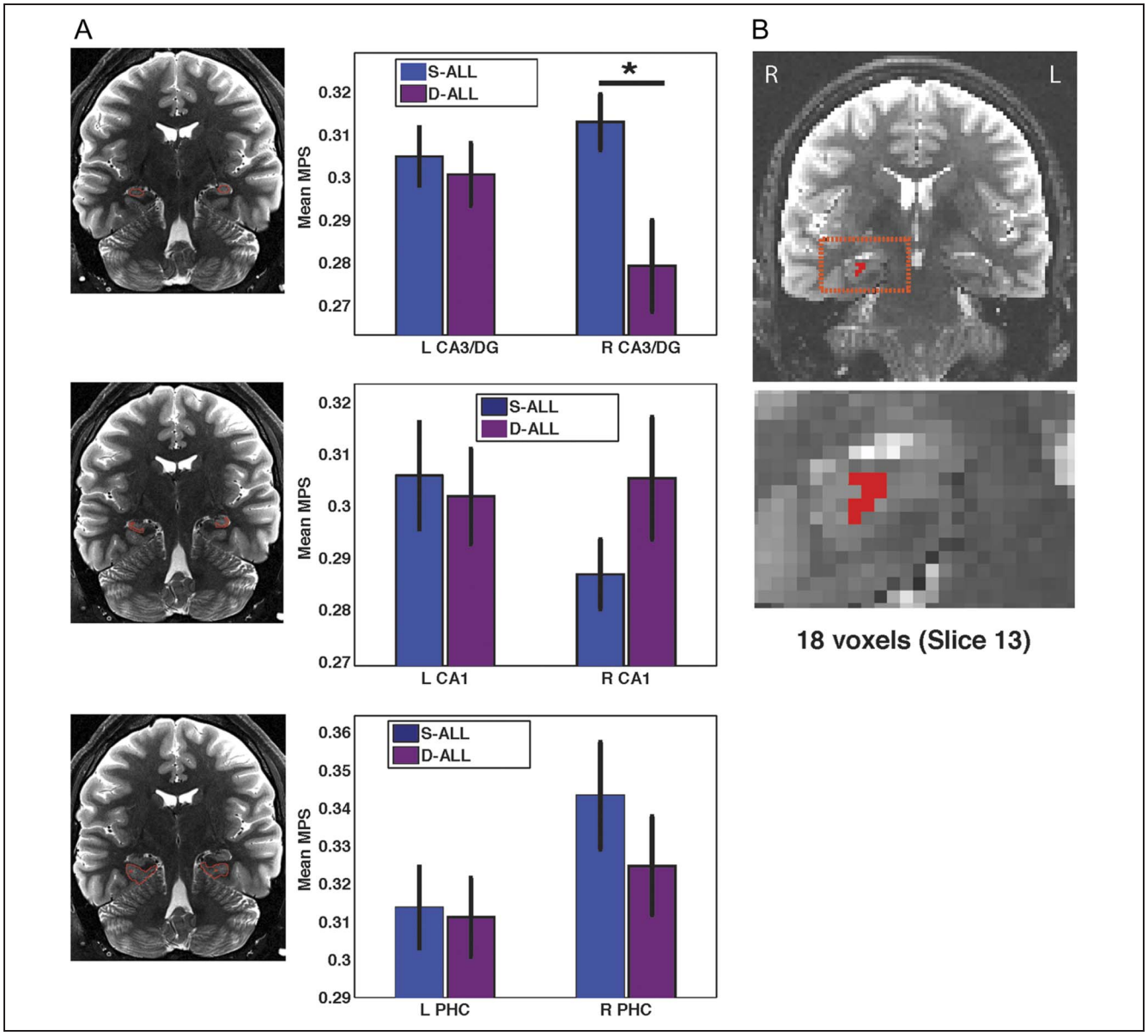

Figure 3. Role for CA3/DG in the differentiation of same versus different trials. (A) When viewing videos of city navigation, S-ALL MPS was significantly greater than D-ALL within the right CA3/DG subregion. (B) A parallel searchlight analysis identified a cluster within right CA3/DG. L = left; R = right.

function of geometric similarity, right CA3/DG (Figure 3A). A repeated-measures ANOVA with factors of Hemisphere (2: left and right), Subfield (3: CA3/DG, CA1, and PHC), and Condition (2: same vs. different trials) revealed a significant main effect of Subfield ($F(3, 45) = 4.79, p < .01$) and a significant Hemisphere × Subfield × Condition interaction ($F(3, 45) = 4.00, p < .05$). Critically, this interaction was not driven by performance; controlling for individual differences in performance, by including map-drawing MDI scores as a covariate in an ANCOVA, produced a comparable Hemisphere × Subfield × Condition interaction effect ($F(2, 28) = 4.06, p < .05$). Post hoc t tests revealed that mean pattern similarity for same trials (S-ALL) was significantly greater than mean MPS for different trials (D-ALL) within right CA3/DG ($t(15) = 2.63, p < .05$) but not within left CA3/DG, bilateral PHC, or bilateral CA1. Furthermore, we found that these MPS differences were not related to univariate parameter estimates. An ANOVA revealed a main effect of subfield ($F(2, 30) = 39.8, p < .0001$), with parameter estimates higher overall in parahippocampal gyrus than hippocampus proper; although unlike MPS effects, no condition-related univariate interaction effects reached significance. Furthermore, no other univariate effects were significant in this analysis (see Supplementary Table 1 for more details). Again, including only correct trials in this analysis yielded similar results.

As an additional means of assessing subfield-specific changes in pattern similarity, we conducted a searchlight

analysis (Kriegeskorte et al., 2006) throughout the MTL, which allowed us to localize fine-scale multivariate patterns. This analysis identified two clusters in CA3/DG: an 18-voxel cluster localized within the right CA3/DG (max t value = 3.49; Figure 3B) exhibiting greater pattern similarity for S-ALL compared with D-ALL trials and a second, smaller cluster within left CA3 also showing S-ALL > D-ALL pattern similarity (maximum t value = 3.04, seven voxels). Overall, these results suggest that CA3/DG activation patterns code for changes in city geometry; when participants viewed the same city, pattern similarity was higher CA3/DG than when they viewed different cities. Furthermore, our analyses revealed that these effects could not be accounted for by differences in participant performance or univariate effects alone.

Differences in Pattern Similarity as a Function of Contextual Input

To better understand whether changes in CA3/DG scaled with parametric changes in spatial context, we compared different trials based on those that differed by a single city iteration (D-1) versus two city iterations (D-2; see Figure 2A). On the basis of our findings of higher MPS for same versus different trials in right CA3/DG, we conducted a repeated-measures ANOVA focusing specifically within

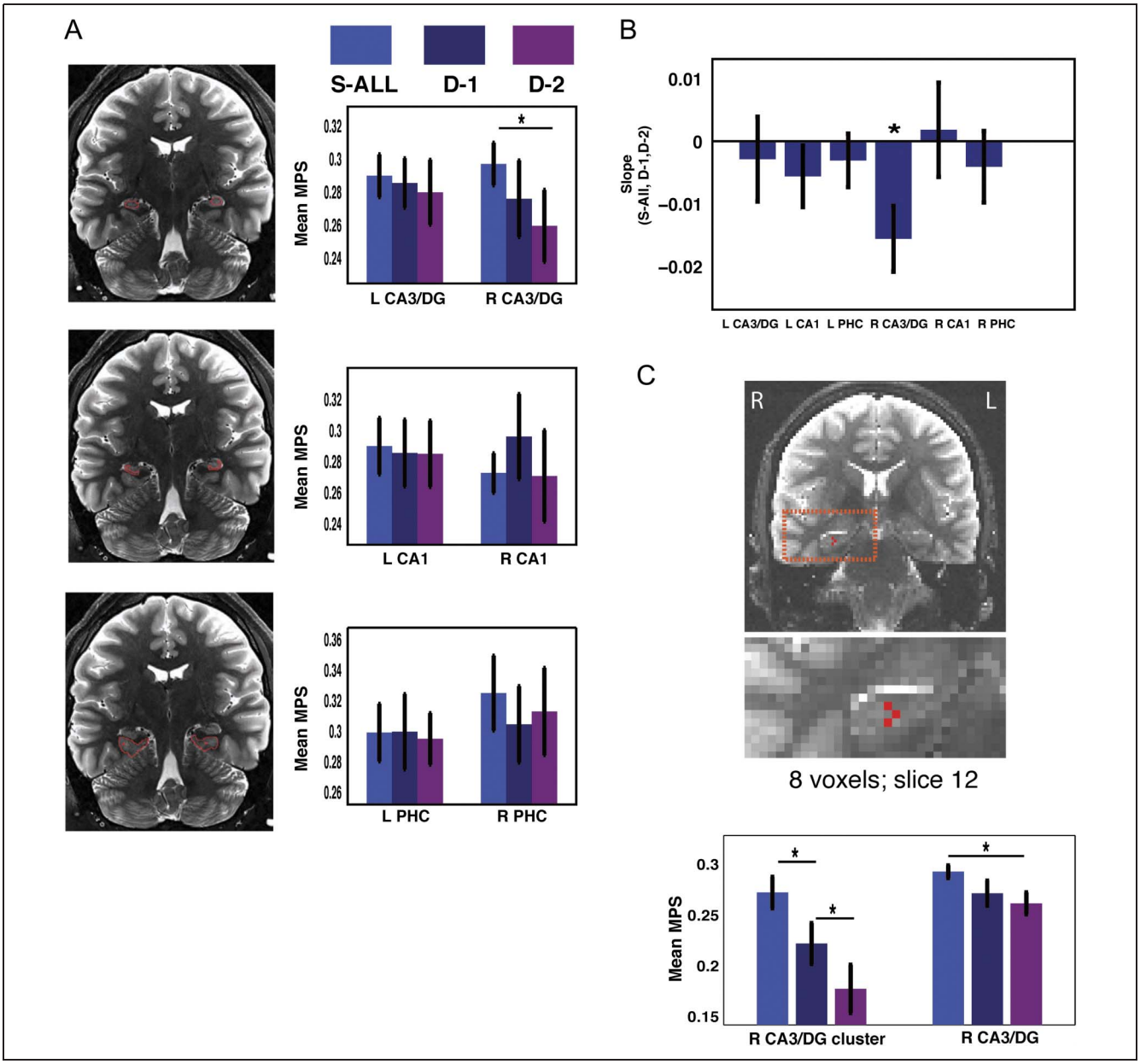

Figure 4. CA3/DG response scales parametrically with city dissimilarity. (A) MPS response scales with changes in city geometry, an effect localized to the CA3/DG subregion. (B) Slope of S-ALL, D-1, and D-2 was significant across all participants. (C) Searchlight linear trend analysis identified a cluster within right CA3/DG. L = left; R = right.

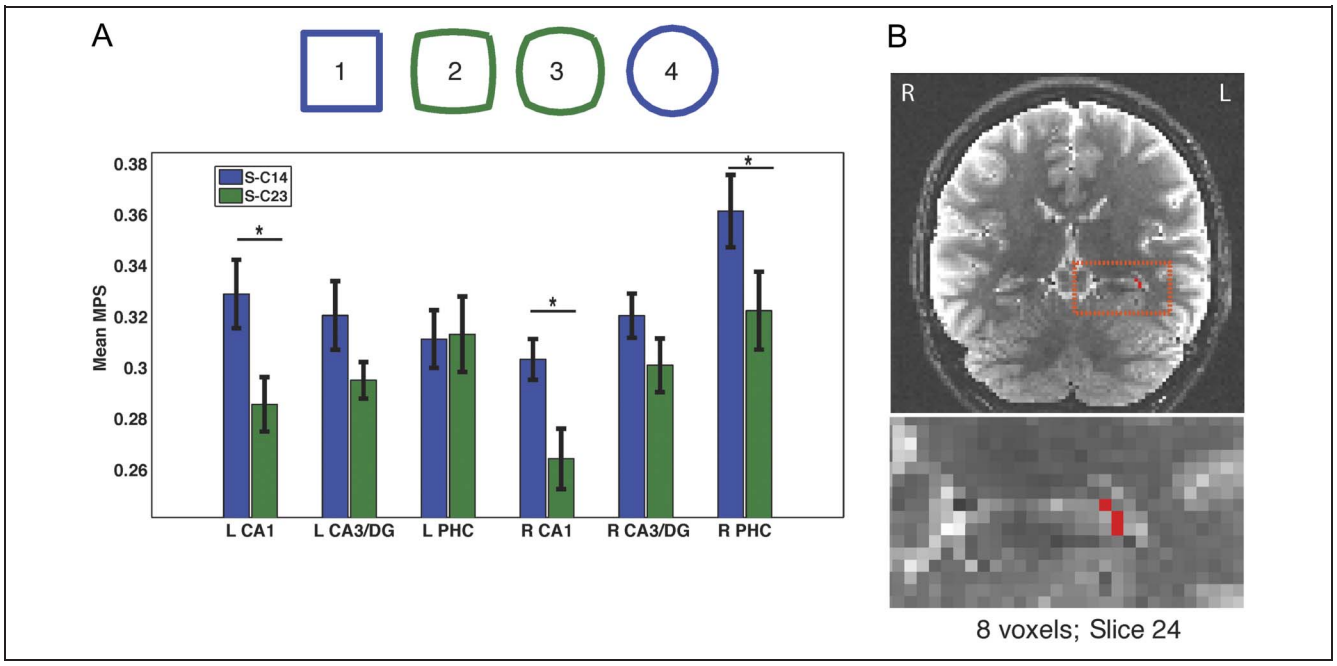

Figure 5. CA1 response to regular compared with morphed city shapes. (A) CA1 and right PHC showed higher MPS than CA3/DG for regular compared with morphed cities. (B) In support of the ROI analysis, our searchlight analysis revealed an eight-voxel cluster centered within the left CA1. L = left; R = right.

the right hemisphere with factors of Subfield (CA3/DG, CA1, and PHC) and Condition (S-ALL, D-1, and D-2). We found a significant main effect of Subfield ($F(2, 30) = 9.75, p < .005$) and a significant Subfield × Condition interaction effect (Figure 4A; $F(4, 60) = 3.87, p < .01$). A linear trend analysis revealed a significant decrease in pattern similarity across the three conditions (i.e., same > D-1 > D-2 trials) for CA3/DG ($t(15) = 3.78, p < .005$) but not for other regions (Figure 4B). A searchlight analysis based on the same linear model confirmed these findings, revealing a significant cluster in right CA3/DG (nine voxels; max $t = -2.58$, $p < .05$ [corrected]; Figure 4C) with no other significant clusters. These data suggest that CA3/DG not only exhibited pronounced sensitivity to changes in spatial context but also, more specifically, displayed decreased pattern similarity as a function of geometrical dissimilarity. These findings are consistent with previous findings from rodent work, suggesting that CA3/DG plays a role in differentiating (pattern separating) more dissimilar inputs (i.e., different geometries) and completing overlapping inputs (i.e., the same geometry; for a review, see Yassa & Stark, 2011).

Role for CA1 in Integration of CA3 Input with Cortical Geometric Percepts

Prior theoretical and empirical work suggests that CA1 may integrate cortical input via the temporoammonic path with current input from CA3/DG (Katz et al., 2007; Remondes & Schuman, 2004). As we noted in our behavioral results, map-drawing performance was better for the geometrically regular compared with morph cities, and discrimination performance was higher on trials involving the same city judgments for the geometrically regular cities (i.e., correctly judging whether the video clip involved the same square- or circle-shaped city, termed S-C1&4) compared with trials involving correctly judging the morphed cities as same (S-C2&3; Table 1; Figure 2A). Thus, we hypothesized that geometrically regular cities might be important in anchoring how participants formed representation of both the regular and morphed cities. Past research has demonstrated a bias in inferotemporal cortex toward representing objects as either square or circular (Op de Beeck et al., 2001), whereas PHC is a key node in processing regularities in scene-specific spatial context (Epstein, Harris, Stanley, & Kanwisher, 1999). Because cortical areas communicate directly with CA1 via the temporoammonic pathway (Amaral & Insausti, 1990), we hypothesized that regular geometric shapes stored in cortical areas might interact to a greater extent with CA1 representations for regular cities compared with the morphs. To assess whether subfield ROIs exhibited differential representational sensitivity to city type, we divided the S-ALL condition into two component groups: S-C1&4 (same trials involving the City 1 or City 4, i.e., circle- or square-shaped cities) or S-C2&3 (same trials involving City 2 or City 3, i.e., circle–square morph and square–circle morph trials). A repeated-measures Hemisphere (2) × Subfield (3) × City type (2) ANOVA revealed a significant Hemisphere × Subfield × City type interaction ($F(2, 30) = 4.16, p < .05$; Figure 5A). Importantly, when performing the identical analysis but using univariate parameter estimate

scores, we found no significant main or interaction effects (Subfield × City type: $F(2, 30) = 0.29$, $p = .75$; Hemisphere × Region × City type: $F(2, 30) = 0.26$, $p = .78$; see also Supplementary Table 1). Simple effect comparisons revealed that both left and right CA1 showed significantly higher MPS for S-C1&4 trials when compared with S-C2&3 trials (left CA1: $t(15) = -2.98$, $p < .01$; right CA1: $t(15) = -2.63$, $p < .05$), with right PHC also showing higher MPS for S-C1&4 compared with S-C2&3 ($t(15) = 2.86$, $p < .05$). Neither left nor right CA3/DG demonstrated significantly higher mean MPS scores for S-C1&4 over S-C2&3 (left CA3/DG: $F(1, 14) = 2.01$, $p = .18$; right CA3/DG: $F(1, 14) = 1.15$, $p = .30$). Repeating the same analysis but limited to only correctly judged same trials (rather than all trials) did not change our results. Furthermore, a follow-up searchlight analysis converged with the above ROI analysis by revealing a cluster primarily within the left CA1 subfield showing higher MPS for regular compared with morph cities (maximum t value = 4.00, eight voxel cluster; Figure 5B).

Overall, our results showed that MPS was greater for geometrically regular cities (Cities 1 and 4) compared with the morphs (Cities 2 and 3), an effect primarily restricted to CA1. These results confirm that trial-by-trial representational patterns within CA1 were particularly sensitive to regular geometric percepts, suggesting a bias in CA1, but not CA3/DG, toward more stable representations for the regular geometric cities compared with the morphs. Importantly, these findings could not be accounted for by differences in performance nor univariate activation patterns alone.

CA1 Shows Increased Pattern Similarity Coherence with PHC for Regular Compared with Morphed Cities

Our results above suggest that CA1 exhibits a possible relationship with long-term stored contextual frames by representing, more strongly, regular compared with morphed spatial contexts. Critical to determining whether this input might come via the temporoammonic pathway involves showing greater interactions between CA1 and cortical areas, such as PHC, during processing of the regular compared with morphed cities. To test this idea, we analyzed IRPC—essentially, the covariation of pattern similarity between brain regions—during regular and morphed same city trials. A repeated-measures ANOVA with factors condition (S-C1&4 and S-C2&3) and seed region (left CA1, left CA3/DG, right CA1, and right CA3/DG) revealed a significant main effect of seed region ($F(1, 15) = 21.96$, $p < .001$) and a Condition × Seed region interaction effect (Figure 6A and B; $F(1, 15) = 8.37$, $p < .05$). Post hoc comparisons revealed that this interaction effect was driven, in part, by the fact that right CA1 exhibited greater IRPC with right PHC for S-C1&4 trials than S-C2&3 ($t(15) = 3.17$, $p < .01$). This finding suggested that CA1 displayed significantly higher coherence with PHC on regular compared with morphed city trials. Whereas post hoc comparisons revealed that CA3/DG–CA1 coherence exceeded both CA3/DG–PHC ($t(15) = 2.52$, $p = .02$) and CA1–PHC ($t(15) = 4.41$, $p \leq .001$), there was no difference between conditions for CA3/DG–CA1 connectivity ($t(15) = -0.93$, $p = .36$). It should be noted that we employed only correct trials in our analysis because

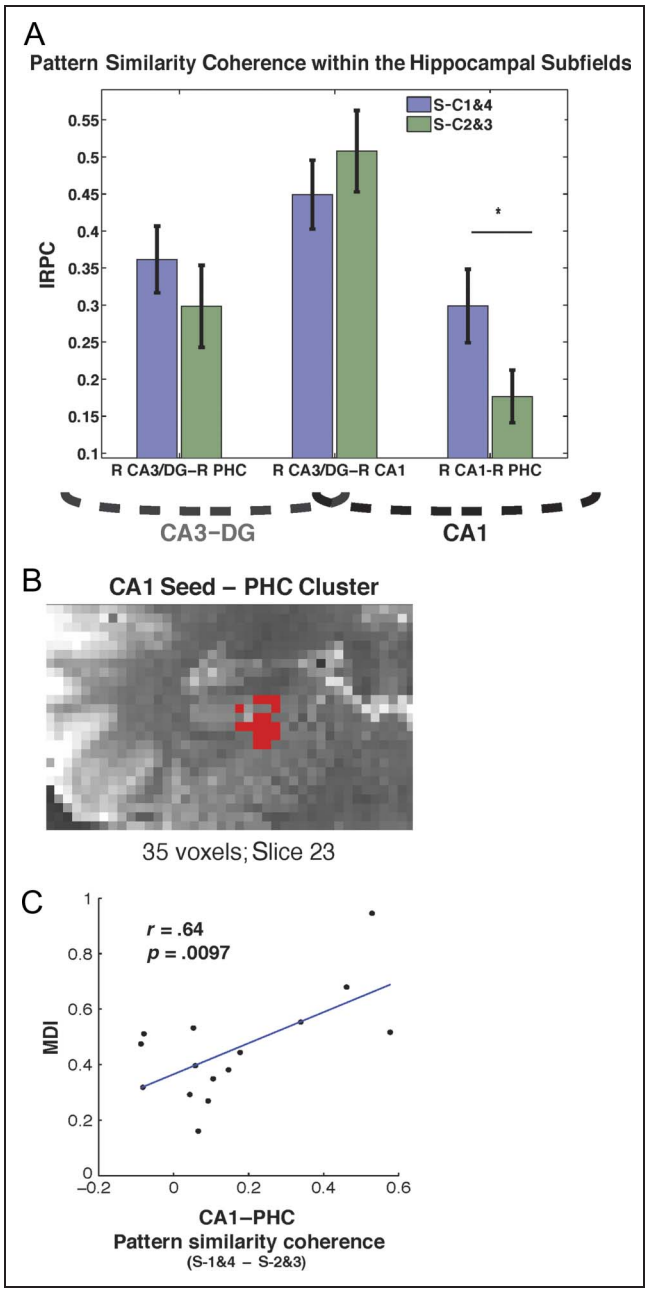

Figure 6. Correlation between CA1 and PHC responses for regular compared with morphed cities. (A) CA1–PHC exhibited greater interregional coherence during S-C1&4 trials than for morphed trials. (B) A seed-based searchlight coherence analysis, contrasting S-C1&4 with S-C2&3 coherence, yielded similar results, revealing a 35-voxel cluster in the right PHC. (C) Higher CA1–PHC interregional coherence predicted worse overall map-drawing performance across participants. L = left; R = right.

of increased signal to noise for correct compared with incorrect responses, which could be a greater factor influencing interregional effects. Employing all trials (correct and incorrect), as we did in other analyses, led to similar overall results (significant Subregion × Condition interaction, $F(1, 15) = 5.87, p < .05$).

Past studies have also suggested that morphed spatial environments may result in "hysteresis" of hippocampal representations such that those for morphed shapes may lag somewhat behind those of the more salient shapes (Leutgeb et al., 2005). In the same fashion that strong schematic labels can lead to worse memory performance (Brod, Werkle-Bergner, & Shing, 2013; Sloutsky & Fisher, 2004), this idea would predict that participants exhibiting higher MPS for the regular shapes (square and circle) might encode less accurate map details because of an inability to suppress the more rigid template representations. Conversely, it may be that strong representations of the regular shapes augment allocentric representation integration and therefore effectively improve map-drawing accuracy. To address these competing possibilities, we correlated map-drawing scores (i.e., participant map-drawing distortion indices) with S-C1&4 versus S-C2&3 IRPC for right CA1–PHC. We found that right CA1–PHC coherence significantly correlated with map-drawing performance ($r = .64, p < .01$; Figure 6C) such that greater CA1–PHC IRPC predicted overall poorer map recall. Interestingly, we did not find a significant correlation between map-drawing performance and S-C1&4 versus S-C2&3 MPS within either left or right CA1, although we did observe a trending relationship within right PHC ($r = .44, p = .09$). Taken together, our results suggest that neocortical–CA1 interactions (via PHC) play a potential role in communicating geometrical templates, perhaps to integrate new traces embodying novel contextual representations.

DISCUSSION

On the basis of past anatomical tracing work (Cenquizca & Swanson, 2007; Amaral & Insausti, 1990) and computational models of hippocampal subfield function (Katz et al., 2007; Levy, 1989), we hypothesized that CA3/DG and CA1 subfields of the hippocampus would show functional differences reflecting their theoretical contributions to episodic memory and navigation. Using a novel measure of representational change within the hippocampal subfields, we found that the right CA3/DG subfield was sensitive to changes in spatial–contextual input (Figure 3). Our results also showed that the CA3/DG region exhibited a graded response pattern, with the degree of MPS scaling with spatial dissimilarity. Thus, as the spatial environments became more dissimilar, right CA3/DG MPS decreased in parallel (Figure 4). Although past studies in humans have suggested a role for CA3/DG in the differentiation of more or less similar visual stimuli during an object recognition task (Azab, Stark, & Stark, 2014; Yassa & Stark, 2011; Lacy et al., 2010; Bakker et al., 2008), our results provide a critical extension to these findings by showing that parametric changes in spatial geometry result in comparable changes to patterns of activation within CA3/DG. These findings are overall compatible with a pattern completion/pattern separation perspective on CA3/DG function because same trials showed a higher degree of pattern similarity (pattern completion) than different trials. In contrast, cities involving different geometries showed increasingly lower pattern similarity (pattern separation), consistent with a role for CA3/DG in both processes (Yassa & Stark, 2011; Guzowski et al., 2004).

In CA1, where we did not observe sensitivity to trial-by-trial change in spatial context, we did find significant MPS differences when participants viewed the same regular geometric city compared with the same morphed city. Our task involved four different cities: two of these cities (Cities 1 and 4) were regular shapes (circle and square), whereas the other two cities (Cities 2 and 3) were morphed versions such that City 2 was closer in shape to City 1 and City 3 was closer in shape to City 4. Comparing same trials involving Cities 1 and 4 to same trials involving Cities 2 and 3 revealed significantly higher similarity of hippocampal representation during the processing of regular shapes within the left and right CA1 subfields. One possible explanation for the increase in MPS for geometrically regular cities is that, in order for the hippocampus to integrate spatial information into stable, recollectable maps, it may be advantageous to integrate this information with task-relevant sensory features, such as stored geometric templates (i.e., squares and circles).

We found further support for the interpretation that CA1 might be playing a role in integrating shape templates with input from CA3/DG using an interregional pattern similarity analyses. This analysis revealed that CA1–PHC IRPS was significantly greater for the regular compared with the morphed cities, which might be expected if cortically stored shape information were input via the temporoammonic pathway. In contrast, although CA3/DG–CA1 IRPS was higher overall than that observed for CA1–PHC, IRPS was not higher for regular versus morphed city recognition judgments in CA3/DG–CA1 (or any other subfield–subfield comparisons), suggesting that CA3–CA1 likely interacted in a condition-independent fashion during spatial recognition. Consistent with a role in integrating cortically stored shape information with existing information actively being processed within the hippocampal circuit, the CA1 subfield is uniquely positioned to receive both direct input from EC via the temporoammonic path as well as direct input from CA3 (Witter, 1993; Amaral & Witter, 1989). Highlighting the relevance of this pathway, Brun and colleagues showed that, even in the absence of CA3 input to CA1 (after CA3 lesions in rodents), direct perforant path input is sufficient to generate stable place fields (Brun et al., 2008). This suggests that cortical input into CA1 may serve as a primary source of spatial information (Brun et al., 2002, 2008). How would this lead

to the emergence of CA1 versus CA3 representational differences? Compared with CA3 cells, which are biased toward coding for the immediate spatial environment, CA1 cells more flexibly code for a broader array of task-relevant features, such as the addition of nonspatial features (Eichenbaum, Dudchenko, Wood, Shapiro, & Tanila, 1999). Rodent remapping studies show that CA3 cells respond more "coherently" to contextual manipulation than CA1 cells (Lee, Yoganarasimha, Rao, & Knierim, 2004; Leutgeb, Leutgeb, Treves, Moser, & Moser, 2004; Vazdarjanova & Guzowski, 2004). In contrast, CA1 cells display properties indicative of a distinctly conjunctive coding scheme. For example, neurons within CA1, when compared with CA3, are more likely to possess multiple place fields (Muller & Kubie, 1987), and remapping studies suggest that CA1 may be more sensitive to common features across environments as opposed to global contextual differences between environments (Leutgeb et al., 2004). In addition, recent work in both rodents and humans has implicated the CA1 field in the process of assimilating new information into prior memories (Larkin, Lykken, Tye, Wickelgren, & Frank, 2014; Schlichting, Zeithamova, & Preston, 2014). These findings are again consistent with a role for CA1 in extracting common features across stimuli, which, based on our results, we suggest may occur via anchoring of pre-existing representational "schemas" such as specific shapes (Tse et al., 2007).

Additional evidence highlighting the importance of neocortical–CA1 connectivity comes from recent navigation studies that suggest a role for retrosplenial cortex and PHC, rather than hippocampus, in accurate map drawing after exploration of a route (Zhang, Copara, & Ekstrom, 2012; Wolbers & Buchel, 2005). Furthermore, recent high-resolution imaging has also suggested that the CA1 subfield and neocortical–CA1 connectivity are important to memory retrieval success (Brown et al., 2014; Duncan et al., 2014). Because CA1 area receives input from PHC via EC and the temporoammonic pathway (Amaral & Insausti, 1990), one possibility is that CA1 may play a role in anchoring new visuospatial input onto existing templates (see also Leutgeb et al., 2005; Remondes & Schuman, 2004), referred to as schemas (van Kesteren et al., 2012; Tse et al., 2007). This schema information, depending on the experimental paradigm, may be primarily verbal, object oriented, or a combination of the two. Consistent with this idea, we note that the squares and circles used in our paradigm would tap into an existing verbal code compared with the morphs. Thus, across both verbal and more visually–spatially oriented paradigms, interactions with cortical areas, including retrosplenial cortex, PHC, and/or pFC, could facilitate input of neural instantiations of schemas into CA1 (McKenzie, Robinson, Herrera, Churchill, & Eichenbaum, 2013; van Kesteren et al., 2012). This opens the possibility, however, that the cortically influenced CA1 code may compete with the spatially constrained CA3 input. Consistent with this idea, we observed worse map-drawing performance in participants with higher CA1–PHC IRPC, suggesting that cortical input may, in some instances, compete with the processed spatial representation received from CA3.

One important caveat is that, although our coherence metric, IRPC, suggests that CA1 and PHC showed similar levels of increases and decreases in pattern similarity across conditions, it does not imply directionality (e.g., that PHC is driving CA1 effects). Nor does it provide direct insight into whether either CA1 or PHC plays a greater role in representing geometrically regular shapes. Past literature, however, shows that patients with hippocampal damage are unimpaired at remembering and drawing simple shapes (Baddeley, Allen, & Vargha-Khadem, 2010; Corkin, 2002), although impaired at representing novel, complex shapes (Jones-Gotman, 1986). Monkey electrophysiological studies further suggest that regular shapes may be stored in inferotemporal cortex (i.e., Op de Beeck et al., 2001), and as outlined above, past literature supports the idea that important aspects of geometric representation (i.e., grid cell representations) are communicated to CA1 via ERC and the temporoammonic pathway (Brun et al., 2008). Thus, based on these findings, we favor the interpretation that shape representations in CA1 are inherited from cortical areas via PHC and the temporoammonic pathway, although our IRPC results themselves cannot speak directly to this issue.

The CA1 region has also been characterized as serving a role in match–mismatch detection to novel input patterns (Kumaran & Maguire, 2006; Lisman, 1999). Several imaging studies have provided support for such models based on evidence of BOLD amplitude changes within CA1 (Duncan, Ketz, Inati, & Davachi, 2012; Dudukovic, Preston, Archie, Glover, & Wagner, 2011). Our findings did not reveal significant differences in mean signal changes (parameter estimates) as a function of condition within CA1 or any other subfield, although our paradigm differs from these prior studies in that it did not involve the quick presentation of series of verbalizable stimuli. We also did not explicitly probe an explicit expectation response as was done previously, which could be important to detecting match- or mismatch-related signals in CA1. Instead, we used a virtual reality paradigm to simulate realistic and quantifiable manipulations specifically focused on spatial context, using stimuli made up of 20-sec-long video clips. Interestingly, our CA3/DG effect, which showed lower MPS for parametrically different, geometrically shaped cities, might, in principle, align better with a match–mismatch process. This interpretation finds support from models arguing that CA3 may be similarly capable of match–mismatch detection given that it receives converging inputs from DG and EC via the perforant path (Vinogradova, 2001; Mizumori & Leutgeb, 1999). Future studies involving direct comparison of object versus spatial context processing using imaging techniques capable of resolving subfield function will be needed to fully address this issue.

Prior imaging studies in humans have reported activation differences between CA3 and CA1 in terms of their

contributions to linear versus nonlinear response signals during sensory processing (Lacy et al., 2010; Bakker et al., 2008). These results, and subsequent computational models, suggest that CA3 demonstrates a pattern completion response in the face of relatively small changes in input, whereas in response to more explicit alterations, CA3 demonstrates a pattern separation response. In addition, these prior imaging studies (Lacy et al., 2010; Bakker et al., 2008) argue that CA1, like CA3/DG, plays a role in completion and separation but displays a more graded, linear response compared with CA3/DG. Whereas we did find separation/completion effects in CA3/DG, we did not find clear pattern separation/completion effects within CA1. However, this previous work utilized an experimental design that involved rapidly presented novel, identical, and familiar lure pictures of objects to participants in the scanner. In contrast, the current virtual reality paradigm required participants to discriminate spatial context during a relatively long period of exploration, which required participants to process distributed spatial features from different viewpoints and reach a subjective threshold to allow for a discrimination-based response. A possible advantage of using geometrical cities is that this method allows clear parameterizing of "sameness" or "differentness." This paradigm is also more comparable with prior rodent studies involving morphed shapes, with MPS bearing more similarity to cellular remapping than the BOLD adaptation technique used in the aforementioned imaging studies. Yet, as mentioned above, coding of objects and otherwise verbalizable material may lead to different representational properties in the hippocampus than spatial context, consistent with some proposals that verbal and spatial materials are handled differently within the hippocampal circuitry (Igloi, Doeller, Berthoz, Rondi-Reig, & Burgess, 2010). Furthermore, rodent studies suggest that distinct pathways involving medial and lateral EC, respectively, handle spatial and nonspatial information inputs into the hippocampus (Hargreaves et al., 2005). This suggests the possibility that these inputs may subsequently be processed differently within the hippocampal circuitry. Again, future studies involving direct comparison of object versus spatial context processing using imaging techniques capable of resolving subfield function will be needed to fully address this issue.

Overall, our results suggest that specific subfields of the hippocampus process distinctive dimensions of information. CA3/DG codes dynamically changing spatial contextual features, whereas CA1, because of its position downstream from CA3 and relative absence of recurrent connectivity, is better suited to integrate context-specific spatial features with stored mnemonic input. Our findings weigh in on the outstanding question regarding the fundamental purpose of the temporoammonic pathway, which connects layer 3 of the EC to CA1, by suggesting a distinct role for CA1 in the integration of CA3 input with cortical representation. Our results thus provide new insight into how the human hippocampal subfields differentially contribute to episodic memory.

Acknowledgments

This work was supported by NINDS R01NS076856, the Sloan Foundation, and the Hellman Young Investigator Award. We thank the UC-Davis memory group for comments on this manuscript.

Reprint requests should be sent to Dr. Arne D. Ekstrom, Center for Neuroscience, University of California, Davis, 1544 Newton Court, Davis, CA 95618, or via e-mail: adekstrom@ucdavis.edu.

REFERENCES

Amaral, D. G., & Insausti, R. (1990). The hippocampal formation. In G. Paxinos (Ed.), *The human nervous system* (pp. 711–755). San Diego, CA: Academic Press.

Amaral, D. G., & Witter, M. P. (1989). The three-dimensional organization of the hippocampal formation: A review of anatomical data. *Neuroscience, 31,* 571–591.

Astur, R. S., Taylor, L. B., Mamelak, A. N., Philpott, L., & Sutherland, R. J. (2002). Humans with hippocampus damage display severe spatial memory impairments in a virtual Morris water task. *Behavioural Brain Research, 132,* 77–84.

Avants, B. B., Epstein, C. L., Grossman, M., & Gee, J. C. (2008). Symmetric diffeomorphic image registration with cross-correlation: Evaluating automated labeling of elderly and neurodegenerative brain. *Medical Image Analysis, 12,* 26–41.

Azab, M., Stark, S. M., & Stark, C. E. (2014). Contributions of human hippocampal subfields to spatial and temporal pattern separation. *Hippocampus, 24,* 293–302.

Baddeley, A., Allen, R., & Vargha-Khadem, F. (2010). Is the hippocampus necessary for visual and verbal binding in working memory? *Neuropsychologia, 48,* 1089–1095.

Bakker, A., Kirwan, C. B., Miller, M., & Stark, C. E. (2008). Pattern separation in the human hippocampal CA3 and dentate gyrus. *Science, 319,* 1640–1642.

Barense, M. D., Henson, R. N., Lee, A. C., & Graham, K. S. (2010). Medial temporal lobe activity during complex discrimination of faces, objects, and scenes: Effects of viewpoint. *Hippocampus, 20,* 389–401.

Brod, G., Werkle-Bergner, M., & Shing, Y. L. (2013). The influence of prior knowledge on memory: A developmental cognitive neuroscience perspective. *Frontiers in Behavioral Neuroscience, 7,* 139.

Brown, T. I., Hasselmo, M. E., & Stern, C. E. (2014). A high-resolution study of hippocampal and medial temporal lobe correlates of spatial context and prospective overlapping route memory. *Hippocampus, 24,* 819–839.

Brun, V. H., Leutgeb, S., Wu, H. Q., Schwarcz, R., Witter, M. P., Moser, E. I., et al. (2008). Impaired spatial representation in CA1 after lesion of direct input from entorhinal cortex. *Neuron, 57,* 290–302.

Brun, V. H., Otnass, M. K., Molden, S., Steffenach, H. A., Witter, M. P., Moser, M. B., et al. (2002). Place cells and place recognition maintained by direct entorhinal–hippocampal circuitry. *Science, 296,* 2243–2246.

Cenquizca, L. A., & Swanson, L. W. (2007). Spatial organization of direct hippocampal field CA1 axonal projections to the rest of the cerebral cortex. *Brain Research Reviews, 56,* 1–26.

Chen, J., Olsen, R. K., Preston, A. R., Glover, G. H., & Wagner, A. D. (2011). Associative retrieval processes in the human medial temporal lobe: Hippocampal retrieval success and CA1 mismatch detection. *Learning and Memory, 18,* 523–528.

Corkin, S. (2002). What's new with the amnesic patient H.M.? *Nature Reviews Neuroscience, 3,* 153–160.

Diana, R. A., Yonelinas, A. P., & Ranganath, C. (2007). Imaging recollection and familiarity in the medial temporal lobe: A three-component model. *Trends in Cognitive Sciences, 11,* 379–386.

Dudukovic, N. M., Preston, A. R., Archie, J. J., Glover, G. H., & Wagner, A. D. (2011). High-resolution fMRI reveals match enhancement and attentional modulation in the human medial temporal lobe. *Journal of Cognitive Neuroscience, 23,* 670–682.

Duncan, K., Ketz, N., Inati, S. J., & Davachi, L. (2012). Evidence for area CA1 as a match/mismatch detector: A high-resolution fMRI study of the human hippocampus. *Hippocampus, 22,* 389–398.

Duncan, K., Tompary, A., & Davachi, L. (2014). Associative encoding and retrieval are predicted by functional connectivity in distinct hippocampal area CA1 pathways. *Journal of Neuroscience, 34,* 11188–11198.

Duvernoy, H. M. (1998). *The human hippocampus: Functional anatomy, vascularization, and serial sections with MRI*. Berlin: Springer.

Eichenbaum, H., Dudchenko, P., Wood, E., Shapiro, M., & Tanila, H. (1999). The hippocampus, memory, and place cells: Is it spatial memory or a memory space? *Neuron, 23,* 209–226.

Eichenbaum, H., Yonelinas, A. P., & Ranganath, C. (2007). The medial temporal lobe and recognition memory. *Annual Review of Neuroscience, 30,* 123–152.

Ekstrom, A. D., Bazih, A. J., Suthana, N. A., Al-Hakim, R., Ogura, K., Zeineh, M., et al. (2009). Advances in high-resolution imaging and computational unfolding of the human hippocampus. *Neuroimage, 19,* 19.

Epstein, R., Harris, A., Stanley, D., & Kanwisher, N. (1999). The parahippocampal place area: Recognition, navigation, or encoding? *Neuron, 23,* 115–125.

Fischer, R. A. (1928). The general sampling distribution of the multiple correlation coefficient. *Proceedings of the Royal Society of Mathematical, Physical, and Engineering Sciences A, 121,* 654–673.

Forman, S. D., Cohen, J. D., Fitzgerald, M., Eddy, W. F., Mintun, M. A., & Noll, D. C. (1995). Improved assessment of significant activation in functional magnetic resonance imaging (fMRI): Use of a cluster-size threshold. *Magnetic Resonance in Medicine, 33,* 636–647.

Graham, K. S., Scahill, V. L., Hornberger, M., Barense, M. D., Lee, A. C., Bussey, T. J., et al. (2006). Abnormal categorization and perceptual learning in patients with hippocampal damage. *Journal of Neuroscience, 26,* 7547–7554.

Guzowski, J. F., Knierim, J. J., & Moser, E. I. (2004). Ensemble dynamics of hippocampal regions CA3 and CA1. *Neuron, 44,* 581–584.

Hargreaves, E. L., Rao, G., Lee, I., & Knierim, J. J. (2005). Major dissociation between medial and lateral entorhinal input to dorsal hippocampus. *Science, 308,* 1792–1794.

Hartley, T., Bird, C. M., Chan, D., Cipolotti, L., Husain, M., Vargha-Khadem, F., et al. (2007). The hippocampus is required for short-term topographical memory in humans. *Hippocampus, 17,* 34–48.

Igloi, K., Doeller, C. F., Berthoz, A., Rondi-Reig, L., & Burgess, N. (2010). Lateralized human hippocampal activity predicts navigation based on sequence or place memory. *Proceedings of the National Academy of Sciences, U.S.A., 107,* 14466–14471.

Jones-Gotman, M. (1986). Right hippocampal excision impairs learning and recall of a list of abstract designs. *Neuropsychologia, 24,* 659–670.

Katz, Y., Kath, W. L., Spruston, N., & Hasselmo, M. E. (2007). Coincidence detection of place and temporal context in a network model of spiking hippocampal neurons. *PLoS Computational Biology, 3,* e234.

King, J. A., Burgess, N., Hartley, T., Vargha-Khadem, F., & O'Keefe, J. (2002). Human hippocampus and viewpoint dependence in spatial memory. *Hippocampus, 12,* 811–820.

Kirwan, C. B., Jones, C. K., Miller, M. I., & Stark, C. E. (2007). High-resolution fMRI investigation of the medial temporal lobe. *Human Brain Mapping, 28,* 959–966.

Kriegeskorte, N., & Bandettini, P. (2007). Analyzing for information, not activation, to exploit high-resolution fMRI. *Neuroimage, 38,* 649–662.

Kriegeskorte, N., Goebel, R., & Bandettini, P. (2006). Information-based functional brain mapping. *Proceedings of the National Academy of Sciences, U.S.A., 103,* 3863–3868.

Kumaran, D., & Maguire, E. A. (2006). An unexpected sequence of events: Mismatch detection in the human hippocampus. *PLoS Biology, 4,* e424.

Lacy, J. W., Yassa, M. A., Stark, S. M., Muftuler, L. T., & Stark, C. E. (2010). Distinct pattern separation related transfer functions in human CA3/dentate and CA1 revealed using high-resolution fMRI and variable mnemonic similarity. *Learning and Memory, 18,* 15–18.

Larkin, M. C., Lykken, C., Tye, L. D., Wickelgren, J. G., & Frank, L. M. (2014). Hippocampal output area CA1 broadcasts a generalized novelty signal during an object–place recognition task. *Hippocampus, 24,* 773–783.

LaRocque, K. F., Smith, M. E., Carr, V. A., Witthoft, N., Grill-Spector, K., & Wagner, A. D. (2013). Global similarity and pattern separation in the human medial temporal lobe predict subsequent memory. *Journal of Neuroscience, 33,* 5466–5474.

Lee, I., Yoganarasimha, D., Rao, G., & Knierim, J. J. (2004). Comparison of population coherence of place cells in hippocampal subfields CA1 and CA3. *Nature, 430,* 456–459.

Leutgeb, J. K., Leutgeb, S., Treves, A., Meyer, R., Barnes, C. A., McNaughton, B. L., et al. (2005). Progressive transformation of hippocampal neuronal representations in "morphed" environments. *Neuron, 48,* 345–358.

Leutgeb, S., Leutgeb, J. K., Treves, A., Moser, M. B., & Moser, E. I. (2004). Distinct ensemble codes in hippocampal areas CA3 and CA1. *Science, 305,* 1295–1298.

Levy, W. B. (1989). A computational approach to the hippocampal function. In R. D. Hawkins & G. H. Bower (Eds.), *Computational models of learning in simple neural systems* (pp. 243–305). Orlando, FL: Academic.

Lisman, J. E. (1999). Relating hippocampal circuitry to function: Recall of memory sequences by reciprocal dentate–CA3 interactions. *Neuron, 22,* 233–242.

Macmillan, N. A., & Creelman, D. C. (2005). *Detection theory: A user's guide*. Mahwah, NJ: Erlbaum.

McKenzie, S., Robinson, N. T., Herrera, L., Churchill, J. C., & Eichenbaum, H. (2013). Learning causes reorganization of neuronal firing patterns to represent related experiences within a hippocampal schema. *Journal of Neuroscience, 33,* 10243–10256.

Mizumori, S. J., & Leutgeb, S. (1999). Interpreting neural representations of aged animals. *Hippocampus, 9,* 607–608.

Muller, R. U., & Kubie, J. L. (1987). The effects of changes in the environment on the spatial firing of hippocampal complex-spike cells. *Journal of Neuroscience, 7,* 1951–1968.

Op de Beeck, H., Wagemans, J., & Vogels, R. (2001). Inferotemporal neurons represent low-dimensional configurations of parameterized shapes. *Nature Neuroscience, 4,* 1244–1252.

Remondes, M., & Schuman, E. M. (2004). Role for a cortical input to hippocampal area CA1 in the consolidation of a long-term memory. *Nature, 431,* 699–703.

Rissman, J., Gazzaley, A., & D'Esposito, M. (2004). Measuring functional connectivity during distinct stages of a cognitive task. *Neuroimage, 23,* 752–763.

Ritchey, M., Yonelinas, A. P., & Ranganath, C. (2014). Functional connectivity relationships predict similarities in task activation and pattern information during associative memory encoding. *Journal of Cognitive Neuroscience, 26,* 1085–1099.
Rolls, E. T., & Kesner, R. P. (2006). A computational theory of hippocampal function, and empirical tests of the theory. *Progress in Neurobiology, 79,* 1–48.
Schlichting, M. L., Zeithamova, D., & Preston, A. R. (2014). CA subfield contributions to memory integration and inference. *Hippocampus, 24,* 1248–1260.
Sloutsky, V. M., & Fisher, A. V. (2004). When development and learning decrease memory. Evidence against category-based induction in children. *Psychological Science, 15,* 553–558.
Smith, D. M., & Mizumori, S. J. (2006). Hippocampal place cells, context, and episodic memory. *Hippocampus, 16,* 716–729.
Stark, C. E., & Squire, L. R. (2001). When zero is not zero: The problem of ambiguous baseline conditions in fMRI. *Proceedings of the National Academy of Sciences, U.S.A., 98,* 12760–12766.
Tse, D., Langston, R. F., Kakeyama, M., Bethus, I., Spooner, P. A., Wood, E. R., et al. (2007). Schemas and memory consolidation. *Science, 316,* 76–82.
Tulving, E. (2002). Episodic memory: From mind to brain. *Annual Review of Psychology, 53,* 1–25.
van Kesteren, M. T. R., Ruiter, D. J., Fernandez, G., & Henson, R. N. (2012). How schema and novelty augment memory formation. *Trends in Neurosciences, 35,* 211–219.
Vazdarjanova, A., & Guzowski, J. F. (2004). Differences in hippocampal neuronal population responses to modifications of an environmental context: Evidence for distinct, yet complementary, functions of CA3 and CA1 ensembles. *Journal of Neuroscience, 24,* 6489–6496.
Vinogradova, O. S. (2001). Hippocampus as comparator: Role of the two input and two output systems of the hippocampus in selection and registration of information. *Hippocampus, 11,* 578–598.
Viskontas, I., Knowlton, B., Steinmetz, P. N., & Fried, I. (2006). Differences in mnemonic processing by neurons in the human hippocampus and parahippocampal region. *Journal of Cognitive Neuroscience, 20,* 1654–1662.
Wills, T. J., Lever, C., Cacucci, F., Burgess, N., & O'Keefe, J. (2005). Attractor dynamics in the hippocampal representation of the local environment. *Science, 308,* 873–876.
Witter, M. P. (1993). Organization of the entorhinal–hippocampal system: A review of current anatomical data. *Hippocampus, 3,* 33–44.
Wolbers, T., & Buchel, C. (2005). Dissociable retrosplenial and hippocampal contributions to successful formation of survey representations. *Journal of Neuroscience, 25,* 3333–3340.
Yassa, M. A., & Stark, C. E. (2011). Pattern separation in the hippocampus. *Trends in Neurosciences, 34,* 515–525.
Yonelinas, A. P., Kroll, N. E., Dobbins, I., Lazzara, M., & Knight, R. T. (1998). Recollection and familiarity deficits in amnesia: Convergence of remember–know, process dissociation, and receiver operating characteristic data. *Neuropsychology, 12,* 323–339.
Zeineh, M. M., Engel, S. A., & Bookheimer, S. Y. (2000). Application of cortical unfolding techniques to functional MRI of the human hippocampal region. *Neuroimage, 11,* 668–683.
Zeineh, M. M., Engel, S. A., Thompson, P. M., & Bookheimer, S. Y. (2003). Dynamics of the hippocampus during encoding and retrieval of face–name pairs. *Science, 299,* 577–580.
Zhang, H., Copara, M. S., & Ekstrom, A. D. (2012). Differential recruitment of brain networks following route and cartographic map learning of spatial environments. *PLoS One, 7,* e44886.